



King's Research Portal

DOI:

[10.1038/bjc.2015.166](https://doi.org/10.1038/bjc.2015.166)

Document Version

Publisher's PDF, also known as Version of record

[Link to publication record in King's Research Portal](#)

Citation for published version (APA):

Rajkumar, V., Goh, V. J-L., Siddique, M. M., Robson, M., Boxer, G., Pedley, R. B., & Cook, G. J. R. (2015). Texture analysis of (125)I-A5B7 anti-CEA antibody SPECT differentiates metastatic colorectal cancer model phenotypes and anti-vascular therapy response. *BJC: British Journal of Cancer*, 112, 1882-1887. <https://doi.org/10.1038/bjc.2015.166>

Citing this paper

Please note that where the full-text provided on King's Research Portal is the Author Accepted Manuscript or Post-Print version this may differ from the final Published version. If citing, it is advised that you check and use the publisher's definitive version for pagination, volume/issue, and date of publication details. And where the final published version is provided on the Research Portal, if citing you are again advised to check the publisher's website for any subsequent corrections.

General rights

Copyright and moral rights for the publications made accessible in the Research Portal are retained by the authors and/or other copyright owners and it is a condition of accessing publications that users recognize and abide by the legal requirements associated with these rights.

- Users may download and print one copy of any publication from the Research Portal for the purpose of private study or research.
- You may not further distribute the material or use it for any profit-making activity or commercial gain
- You may freely distribute the URL identifying the publication in the Research Portal

Take down policy

If you believe that this document breaches copyright please contact librarypure@kcl.ac.uk providing details, and we will remove access to the work immediately and investigate your claim.

Keywords: single photon emission computed tomography; ^{125}I -A5B7 anti-CEA antibody; texture analysis; tumour heterogeneity; liver metastases

Texture analysis of ^{125}I -A5B7 anti-CEA antibody SPECT differentiates metastatic colorectal cancer model phenotypes and anti-vascular therapy response

V Rajkumar¹, V Goh², M Siddique², M Robson¹, G Boxer¹, R B Pedley^{1,3} and G J R Cook^{*,2,3}

¹UCL Cancer Institute, University College London, 72 Huntley St, London WC1E 6BT UK and ²Division of Imaging Sciences and Biomedical Engineering, Kings College London, St Thomas' Hospital, Westminster Bridge Road, London SE1 7EH, UK

Background: We aimed to test the ability of texture analysis to differentiate the spatial heterogeneity of ^{125}I -A5B7 anti-carcinoembryonic antigen antibody distribution by nano-single photon emission computed tomography (SPECT) in well-differentiated (SW1222) and poorly differentiated (LS174T) hepatic metastatic colorectal cancer models before and after combretastatin A1 di-phosphate anti-vascular therapy.

Methods: Nano-SPECT imaging was performed following tail vein injection of 20 MBq ^{125}I -A5B7 in control CD1 nude mice (LS174T, $n=3$ and SW1222, $n=4$), and CA1P-treated mice (LS174T, $n=3$; SW1222, $n=4$) with liver metastases. Grey-level co-occurrence matrix textural features (uniformity, homogeneity, entropy and contrast) were calculated in up to three liver metastases in 14 mice from control and treatment groups.

Results: Before treatment, the LS174T metastases ($n=7$) were more heterogeneous than SW1222 metastases ($n=12$) (uniformity, $P=0.028$; homogeneity, $P=0.01$; contrast, $P=0.045$). Following CA1P, LS174T metastases ($n=8$) showed less heterogeneity than untreated LS174T controls (uniformity, $P=0.021$; entropy, $P=0.006$). Combretastatin A1 di-phosphate-treated SW1222 metastases ($n=11$) showed no difference in texture features compared with controls (all $P>0.05$).

Conclusions: Supporting the potential for novel imaging biomarkers, texture analysis of ^{125}I -A5B7 SPECT shows differences in spatial heterogeneity of antibody distribution between well-differentiated (SW1222) and poorly differentiated (LS174T) liver metastases before treatment. Following anti-vascular treatment, LS174T metastases, but not SW1222 metastases, were less heterogeneous.

Complexity in the structure and pathophysiology, both within and between tumours, and the heterogeneity observed in clinical images is well recognised. Features in clinical images are a reflection of the underlying cellular and molecular characteristics of tumours including cell proliferation and metabolism, necrosis, fibrosis, differences in blood flow and angiogenesis, hypoxia and expression of specific receptors and antigens (Lankester *et al*, 2007;

Henriksson *et al*, 2007; Ganeshan *et al*, 2013). Within any medical image, including computed tomography (CT), magnetic resonance imaging, positron emission tomography, single photon emission computed tomography (SPECT) and ultrasound, texture features, describing relationships between grey-level intensity and position of pixels, can be extracted, quantified and linked to underlying biological complexity and heterogeneity (Castellano *et al*, 2004;

*Correspondence: Professor GJR Cook; E-mail: gary.cook@kcl.ac.uk

³RB Pedley and GJR Cook are joint senior authors.

Received 7 February 2015; revised 4 April 2015; accepted 17 April 2015; published online 19 May 2015

© 2015 Cancer Research UK. All rights reserved 0007–0920/15

Asselin *et al*, 2012; Davnall *et al*, 2012; Chicklore *et al*, 2013). The biological processes reflected in image heterogeneity remain hypothetical, but there is growing evidence that the measurement of heterogeneity in medical images by textural analysis may allow better tissue characterisation, image segmentation, and prediction of therapy response and survival (Al-Kadi and Watson, 2008; Eary *et al*, 2008; Yu *et al*, 2009; El Naqa *et al*, 2009; Goh *et al*, 2009; Tixier *et al*, 2011; Goh *et al*, 2011; Cook *et al*, 2013; Parikh *et al*, 2014). Second-order statistical based techniques have been most commonly applied, reflecting the local spatial distribution of voxel values, calculating local features at each voxel within the in-plane image and deriving parameters from the distributions of the local features. A number of texture features can be derived that provide a measure of intralesional heterogeneity (Haralick *et al*, 1973; Tixier *et al*, 2011; Davnall *et al*, 2012).

Single photon emission computed tomography imaging is critical for successful planning and monitoring of antibody-targeted radionuclide imaging and therapy (radioimmunotherapy). For example, imaging with ^{111}In -ibritumomab tiuxetan is used to determine whether there is sufficient and uniform antibody retention within the tumour prior to ^{90}Y -ibritumomab tiuxetan radioimmunotherapy, and ultimately determines eligibility for treatment. Longitudinal SPECT imaging is also used to monitor antibody biodistribution and dosimetry in patients, for example, receiving anti-carcinoembryonic antigen (CEA) ^{131}I -A5B7 antibody in combination with the vascular disrupting agent (VDA), combretastatin A4-phosphate (Meyer *et al*, 2009). Texture analysis would be able to augment current methods by quantifying the heterogeneity of antigen distribution non-invasively with imaging, before and after therapy. This would have utility in future clinical trials, potentially giving insight into the resistance of some tumours to antigen-targeted therapy and providing non-invasive imaging biomarkers of tumour phenotype and therapy response.

In this pre-clinical study, we set out to assess the changes in heterogeneity of CEA expression in ^{125}I -A5B7 SPECT images of two contrasting (well-differentiated and poorly differentiated) human colorectal liver metastatic models, before and after therapy with a VDA, combretastatin A1 di-phosphate (CA1P, OXi4503). This drug produces a rapid reduction in tumour blood flow, leading to massive central necrosis by 24 h, but leaving a viable rim of cells at the periphery, which can continue to grow. Our hypotheses were that texture analysis of ^{125}I -A5B7 antibody distribution by SPECT could reveal different characteristics between the two contrasting tumour models and that differences in textural features would exist between treated and untreated liver metastases. Thus, the aim of the study was to test the ability of texture analysis to differentiate the spatial heterogeneity of ^{125}I -A5B7 anti-CEA antibody distribution by nano-SPECT imaging in well-differentiated (SW1222) and poorly differentiated (LS174T) hepatic metastatic colorectal cancer models before and after CA1P anti-vascular therapy.

MATERIALS AND METHODS

Animal studies. The UK Coordinating Committee on Cancer Research Guidelines for the Welfare of Animals in Experimental Neoplasia and the Animal (Scientific Procedures) Act 1986 were followed for all of the animal experiments (Workman *et al*, 1988). The study was reviewed and approved by the UCL Animal Welfare and Ethical Review Body (AWERB) under project licence 70–309. Food and water was available *ad libitum*, the water containing 0.1% potassium iodide to block thyroid uptake of iodine.

Metastatic liver models. Two CEA-producing, human colorectal adenocarcinoma cell lines, LS174T and SW1222 (El Emir *et al*, 2007),

were used to develop liver metastatic models in female nude CD1 mice (6–8-weeks old, 20–25 g) which were purchased from Charles River and acclimatised for a week prior to initiation of studies. Mice were housed under sterile conditions in individually ventilated cages, fed with standard chow diet and water *ad libitum*, and maintained on an automatic 12 h light cycle at 22–24 °C. These models were selected to provide different pathophysiologicals. The LS174T is a moderate to poorly differentiated tumour, with heterogeneous CEA distribution with greatest expression on perivascular tumour cells. The SW1222 tumour is well-differentiated. Carcinoembryonic antigen expression is mainly restricted to the luminal surface of cells surrounding each gland and presents a more homogeneous pattern than LS174T (El Emir *et al*, 2007).

LS174T and SW1222 cells were grown as an adhesion culture in Eagle's Minimal Essential medium supplemented with 10% FCS, 2 mmol l^{-1} L-glutamine, 1% non-essential amino acids (all media components purchased from PAA Laboratories, Yeovil, UK). Sub-confluent cells in logarithmic growth were trypsinised (Trypsin-EDTA, PAA Laboratories), counted and re-suspended in serum-free medium at the required concentration for setting up the models. Mice were anaesthetised using isoflurane and the abdomen was swabbed using chlorhexidine. Subcutaneous Buprenorphine analgesic was administered locally. The spleen was exteriorised through a vertical 1–1.5 cm subcostal incision in the left abdominal wall. Cells (1×10^6 in 0.1 ml) were injected. After 2–3 min, the splenic vessels were tied off using a suture and the spleen was removed. The inner wound was closed using Vicryl-40 stitches and the outer wound was closed using metal clips, which were removed after 9 days. Three LS174T and four SW1222 bearing mice were used as untreated controls. Three LS174T and four SW1222 bearing mice were treated with the VDA, CA1P.

Drug administration. Combretastatin A1 di-phosphate, provided by OXiGENE (San Francisco, CA, USA), was made up in sterile saline and 10 mg kg^{-1} injected intraperitoneally 48 h before antibody administration.

Antibody radiolabelling. A5B7, a monoclonal anti-CEA antibody (UCB-Celltech, Slough, UK), was used for biodistribution studies. This antibody and its fragments are in regular preclinical and clinical use, and have been extensively used in clinical radioimmunotherapy and combined anti-vascular studies (El Emir *et al*, 2007; Meyer *et al*, 2009). A5B7 was labelled with ^{125}I (Perkin Elmer, Boston, MA, USA) using the Iodogen method as previously described (El Emir *et al*, 2007; Folarin *et al*, 2010). Briefly, ^{125}I and A5B7 were mixed at a ratio of 5:1 in Iodogen tubes (Pierce, Loughborough, UK) for 20 min. The mixture was then loaded onto a PD-10 desalting column (GE Healthcare, Amersham, UK) and radiolabelled antibody was eluted with PBS. Thin layer chromatography was used to assess radiopharmaceutical purity (silica gel Si60, stationary phase and 80% methanol, mobile phase).

Small animal SPECT/CT imaging. LS174T ($n=3$) and SW1222 ($n=4$) tumour-bearing CD1 nude mice were used as untreated controls. LS174T ($n=3$) and SW1222 ($n=4$) mice were treated with CA1P (10 mg kg^{-1} i.p.). After 48 h, the radiolabelled antibody was administered to the mice (0.1 ml in sterile saline, 20 MBq, $25\text{ }\mu\text{g}^{-1}$ protein per mouse) via the tail vein. After a further 48 h the mice were anaesthetised by inhalation of 2% isoflurane in oxygen and imaged with a NanoSPECT/CT small animal imager (Mediso Imaging Systems, Budapest, Hungary) for 2 h using a multi-pinhole (nine pinholes, aperture 1.0 mm collimator and a transaxial FOV of 62 mm). A total of 24 projections were acquired in a 256×256 matrix with a minimum of 10 000 counts per projection. Single photon emission computed tomography images were reconstructed with Hi SPECT software using a dedicated ordered subset-expectation maximisation algorithm (Scivis, Göttingen, Germany). Computed tomography images (240 projections,

1 second, 55 kVp) were acquired prior to SPECT imaging. The SPECT and CT fusion images were obtained using the automatic fusion feature of the InVivoScope software (Bioscan Inc., Washington, D.C., USA).

Texture analysis. Regions of interest were drawn manually around up to three of the largest liver metastases in each of the 14 mice on each transaxial slice of ¹²⁵I-A5B7 SPECT images in which the tumours were visible. Metastases greater than 0.3 cm in diameter were selected to minimise potential partial volume effects on analysis. The range in diameter for the selected lesions was 0.31–1.02 cm (mean = 0.51 cm). Second-order, statistical based texture features were calculated from grey level co-occurrence matrices (GLCM) which measure the grey-level distribution of pairs of voxels (Haralick *et al*, 1973). This method summarises the distribution of neighbouring pairs of voxels in 13 orientations and two directions, the voxel size being 0.3 × 0.3 × 0.3 mm. Calculation of the textural features was performed using in-house software implemented under MATLAB (The MathWorks Inc., Natick, MA, USA). Voxel values within the tumour VOI were resampled to yield 32 discrete bins. Measured parameters included uniformity (also termed angular second moment or energy) and homogeneity, reflecting similarity of intensities between neighbouring voxels (homogeneity parameters) as well as entropy and contrast, reflecting randomness and local variations of voxel distributions, respectively (heterogeneity parameters) (Haralick *et al*, 1973) (see Appendix Table 1 for detail on texture features). These most commonly used second-order features provide additional information on the relationship between voxels compared with global first-order features and have been shown to be robust in terms of reproducibility and predictive ability (Howarth and Ruger, 2004; Tixier *et al*, 2012). In each of the 14 mice, regions of interest definitions and parameter measurements were performed again in a metastasis at a separate time point to assess measurement variability, expressed as intraclass correlation coefficients for each of the four texture features.

Histological analysis and CEA staining. After SPECT imaging, the mice were killed and segments of liver containing metastatic deposits were excised and fixed in 10% neutral buffered formalin for at least 48 h prior to processing and paraffin embedding. Four micrometer-thick tumour sections were stained with haematoxylin and eosin to assess general tumour morphology. Carcinoembryonic antigen immunostaining was performed using a biotinylated version of A5B7 as previously described (El Emir *et al*, 2007). High-resolution composite images of tumour sections were acquired on an Axioimager. Z2 microscope (Carl Zeiss, Cambridge, UK) using TissueFAXS software (TissueGnostics, Vienna, Austria).

Statistical analysis. Statistical analyses were performed using SPSS for Windows version 20 (IBM, Chicago, IL, USA). Differences in textural feature values between untreated LS174T and SW1222 metastases, and between untreated and treated metastases, for both LS174T and SW1222 metastatic models were tested using the Mann-Whitney U test with two tailed significance at 5%.

RESULTS

Tumour size and reproducibility of measurements. No significant difference in mean lesion diameters was found between the two control groups (LS174T mean 0.43 cm, SW1222 mean 0.54 cm, *P* = 0.06) or between control and treated groups (treated LS174T mean 0.49 cm, *P* = 0.82, treated SW1222 mean 0.54 cm, *P* = 0.49). Intraobserver variability (intraclass correlation coefficient, 95% confidence interval) was as follows for each parameter; contrast

(0.94, 0.83–0.98), uniformity (0.98, 0.93–0.99), entropy (0.98, 0.93–0.99) and homogeneity (0.98, 0.94–0.99).

Texture feature analysis

Control mice. In the three untreated LS174T mice, 7 metastases were evaluable, and in the four untreated SW1222 mice, 12 metastases were selected for texture analysis. Grey level co-occurrence matrices measures of local homogeneity (uniformity and homogeneity) were lower in the poorly differentiated control LS174T metastases than in the well-differentiated SW1222 lesions (Table 1). The mean uniformity in LS174T lesions was 0.6 times that of the SW1222 lesions (mean = 0.005 and 0.007 respectively, *P* = 0.028) and the mean homogeneity was 0.8 times that of SW1222 lesions (mean = 0.33 and 0.40, respectively, *P* = 0.01). As a measure of heterogeneity, GLCM contrast was 1.7 times greater in LS174T compared with SW1222 lesions (mean = 31.2 and 18.7, respectively, *P* = 0.045). Grey level co-occurrence matrices entropy was greater in LS174T lesions but this difference did not reach statistical significance (mean = 5.7 and 5.4, respectively, *P* = 0.068).

CA1P-treated mice

LS174T metastases: For the three mice bearing LS174T tumours, which received CA1P treatment, eight metastases were evaluable. In these poorly differentiated lesions, GLCM features of homogeneity were higher following treatment than in untreated mice, although this did not reach statistical significance for the homogeneity parameter (Table 2). The mean uniformity was 2.2 times greater in treated compared with control lesions (mean = 0.01 and 0.005, respectively, *P* = 0.021) and homogeneity

Table 1. GLCM textural features in untreated control LS174T and SW1222 metastases					
GLCM texture feature	LS174T mean	LS174T s.d.	SW1222 mean	SW1222 s.d.	P value
Uniformity	0.005	0.001	0.007	0.004	0.028
Homogeneity	0.33	0.04	0.40	0.07	0.01
Contrast	31.2	12.1	18.7	8.2	0.045
Entropy	5.7	0.2	5.4	0.4	0.068
Abbreviations: GLCM = Grey level co-occurrence matrix; s.d. = standard deviation.					

Table 2. GLCM textural features in CA1P-treated LS174T metastases compared with controls					
GLCM texture feature	LS174T Treated mean	LS174T Treated s.d.	LS174T control mean	LS174T control s.d.	P value
Uniformity	0.01	0.01	0.005	0.001	0.021
Homogeneity	0.39	0.1	0.33	0.04	0.07
Contrast	20.8	12.9	31.2	12.1	0.11
Entropy	5.3	0.4	5.7	0.2	0.006
Abbreviations: GLCM = Grey level co-occurrence matrix; s.d. = standard deviation.					

Table 3. GLCM textural features in CA1P-treated SW1222 metastases compared with controls					
GLCM texture feature	SW1222 Treated mean	SW1222 Treated s.d.	SW1222 control mean	SW1222 control s.d.	P value
Uniformity	0.007	0.004	0.007	0.004	0.38
Homogeneity	0.39	0.09	0.40	0.07	0.41
Contrast	19.1	10.0	18.7	8.2	0.79
Entropy	5.4	0.4	5.4	0.4	0.98
Abbreviations: GLCM = Grey level co-occurrence matrix; s.d. = standard deviation.					

1.2 times that of control lesions (mean = 0.39 and 0.33, respectively, $P = 0.07$). Grey level co-occurrence matrices features of heterogeneity were lower in treated lesions although this was only statistically significant for entropy. The mean entropy in treated lesions was 0.9 times that of control lesions (mean = 5.3 and 5.7, respectively, $P = 0.006$) and contrast 0.7 times that of control lesions (mean = 20.8 and 31.2, respectively, $P = 0.11$).

SW1222 metastases: For the four mice bearing SW1222 tumours, which received CA1P treatment, 11 metastases were selected for texture analysis. In these well differentiated lesions, the treated metastases showed no significant difference in texture of hepatic metastases compared with controls ($n = 12$) for any of the GLCM features (Table 3).

Representative SPECT images of intrahepatic metastases from both SW1222 and LS174T are shown in Figure 1.

Histological analysis. Histological analysis confirmed that control LS174T and SW1222 sections demonstrated a typical morphology and pattern of CEA expression (El Emir *et al*, 2007). SW1222 tumour deposits were organised into highly differentiated viable glandular structures (Figure 2A). Carcinoembryonic antigen expression was limited to the apical surface of cells surrounding each gland and was uniformly expressed throughout the tumour (Figure 2E). LS174T tumours displayed moderate to poor differentiation with little evidence of glandular structures (Figure 2C). Expression of CEA was heterogeneously distributed throughout the tumour, with the expression being most predominant on perivascular tumour cells (Figure 2G). Treatment with CA1P in both SW1222 and LS174T tumours resulted in the development of a central necrotic core with only a peripheral rim of viable tumour cells remaining (Figure 2B and D), which were shown to express CEA (Figure 2F and H).

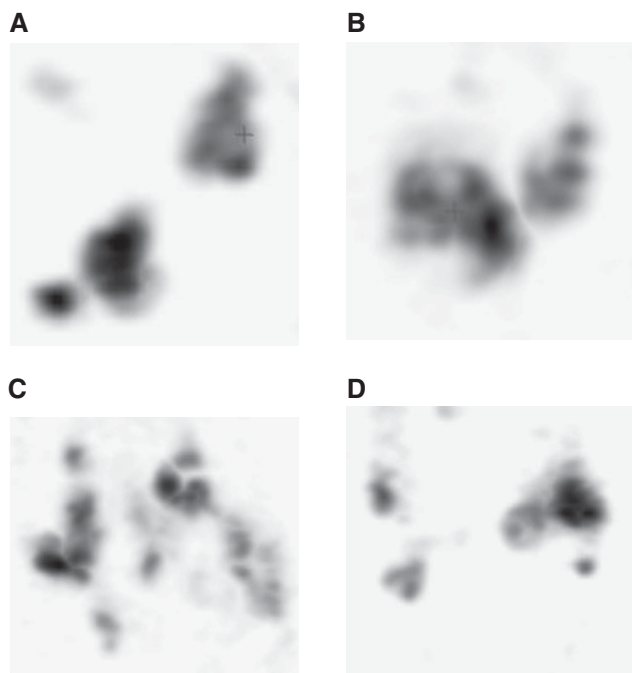


Figure 1. Representative SPECT images showing the distribution of ^{125}I -A5B7 anti-CEA in both control (A) and treated (B) SW1222 and LS174T control (C) and treated (D) intrahepatic metastases. Visual comparison does not reveal obvious differences between tumour types or the effects of treatment.

DISCUSSION

Texture analysis of SPECT images of ^{125}I -A5B7 anti-CEA antibody shows the distribution is more heterogeneous in an untreated poorly differentiated human colorectal metastatic model (LS174T) than in a model with a well-differentiated glandular structure (SW1222). This result is in agreement with previous observations for subcutaneous models of LS174T and SW1222 xenografts when measured by three-dimensional microvascular corrosion casting, high resolution multifluorescence microscopy and transmission electron microscopy (El Emir *et al*, 2007; Folarin *et al*, 2010; Rajkumar *et al*, 2014) which showed that vascular supply, tumour structure and antigen distribution varied greatly between the two models.

Measurement of all texture parameters showed good reproducibility with intraclass correlation coefficients ranging from 0.94 for contrast to 0.98 for uniformity, entropy and homogeneity.

The most relevant factor for our study is the difference in antigen distribution between the two models. In the LS174T model, CEA is distributed very heterogeneously, but with greatest expression on perivascular tumour cells, while in the SW1222 model it is restricted to the luminal surface of the cells making up the well-defined glands, and presents a far more homogeneous pattern than seen in LS174T. Of relevance, the differences in CEA distribution between the two models lead to variances in response to therapeutic ^{131}I -labelled A5B7 antibody, with the more homogeneous distribution of target antigen in SW1222 leading to superior therapeutic effect (El Emir *et al*, 2007). The observations in our study support the ability of image texture analysis to demonstrate and quantify a more uniform distribution of antibody in one tumour model compared with another.

We have demonstrated higher homogeneity (uniformity and homogeneity) and lower heterogeneity (contrast and entropy) of ^{125}I -A5B7 antibody distribution in liver metastases from the poorly differentiated LS174T model treated with the VDA CA1P compared with untreated controls. This mathematical and statistical description, demonstrating a change from a heterogeneous to a more homogeneous antibody distribution following VDA treatment, aligns well with the features observed under the microscope (Figure 2). Following VDA treatment, approximately 90% of the tumour cells are killed (central areas of the lesions becoming extensively necrotic, following vascular haemorrhage), leaving only a rim of viable tumour at the periphery of the deposit. This is thought to be maintained by nutrients from normal blood flow through the sinusoids of the liver. In contrast, the well-differentiated SW1222 model showed no change in measures of heterogeneity of antibody distribution following therapy, compared with untreated tumours. This probably reflects the homogenous nature of local antibody biodistribution in control SW1222 tumours, and similarly the almost entirely necrotic nature of CA1P-treated tumours. Therefore, although the overall antibody distribution in SW1222 tumours is restricted to a very narrow tumour rim (1–2 cell diameters) following CA1P treatment, this is insufficient to alter the output measure of local heterogeneity parameters.

In order to develop this texture analysis approach in clinical practice, there is a need to understand how the tissue structure and cellular architecture observed on microscopy fill the volume of a voxel generated by the clinical imaging modality, and to show how those multiple groups of cells and tissue components generate the relative grey-level intensities. The minimum size of tumour lesion/regions of interest analysed (0.31 cm) consists of approximately 1000 voxels ($10 \times 10 \times 10$) each being $0.3 \times 0.3 \times 0.3$ mm. Within an image, the associated grey-level value for each voxel is the product of multiple types of cell (tumour cells and inflammatory cells), connective tissue stromal elements including vessel walls,

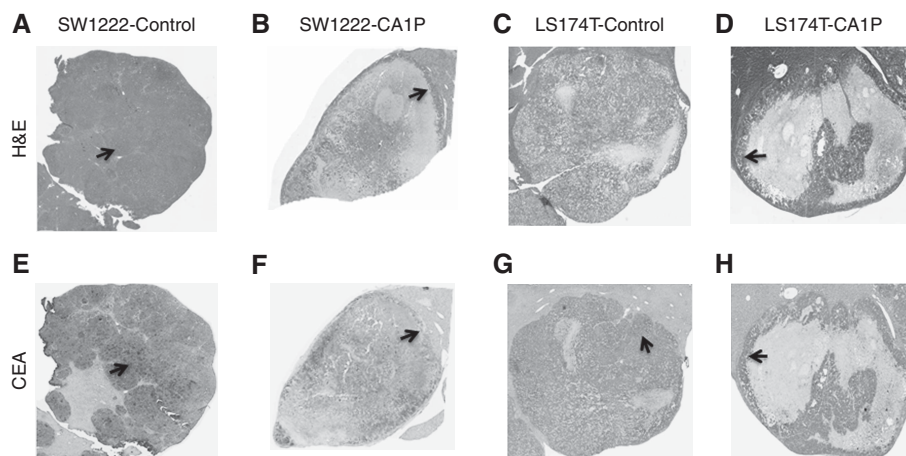


Figure 2. Representative haematoxylin and eosin (**A–D**) and anti-CEA immunohistochemical (**E–H**) micrographs demonstrating the effect of CA1P on the distribution of viable cells and CEA in SW1222 (**A, B, E, F**) and LS174T (**C, D, G, H**) intrahepatic metastases. Control SW1222 metastases are almost totally viable (arrow, **A**), with relatively uniform expression of CEA (arrow, **E**). After treatment with CA1P, viable CEA-expressing tumour cells are restricted to the peripheral rim (arrow, **B** and **F**). In control LS174T metastases (**C**), CEA expression (arrow, **G**) is more heterogeneous than in SW1222 metastases (**E**). After treatment with CA1P (**D**), viable and CEA-expressing tumour cells are similarly restricted to the peripheral rim (arrows, **D** and **H**).

blood, body fluids and water, and for SPECT images, the relative distribution of radiolabelled antibody. The challenge is to develop further our understanding of how these histological features relate to the measurements of voxel grey-level intensity.

It is now well-recognised that radiological images contain more useful information than may be perceived by visual inspection and that additional quantification of imaging texture features, describing the spatial distribution and heterogeneity of voxel intensities, can augment clinical practice. There is also accumulating evidence that parameters obtained by texture analysis, reflecting intratumoural heterogeneity, may yield additional predictive and prognostic information (Al-Kadi and Watson, 2008; Eary *et al*, 2008; El Naqa *et al*, 2009; Yu *et al*, 2009; Goh *et al*, 2009, 2011; Tixier *et al*, 2011; Davnall *et al*, 2012; Chicklore *et al*, 2013; Cook *et al*, 2013; Parikh *et al*, 2014). Our preclinical imaging observations add weight and value to this clinical approach. Both SW1222 and LS174T intrahepatic metastases were readily detected by SPECT imaging, however, VDA-induced changes in antibody distribution could only be confirmed by texture analysis of the SPECT images. To date, the biological correlates of textural features in different types of medical imaging remain largely unknown. It is postulated that increased image heterogeneity within tumours may be associated with differences in regional tumour cellularity, proliferation, hypoxia, angiogenesis and necrosis (Henriksson *et al*, 2007; Ganeshan *et al*, 2013), factors that independently have been associated with more aggressive behaviour, poorer response to treatment and worse prognosis. It is unlikely that structural (e.g., CT, magnetic resonance imaging) and functional (e.g., positron emission tomography, SPECT) imaging textural features are associated with the same biological causes of spatial intensity variations within an image, although in general, features that correspond to increased heterogeneity tend to relate to poor prognosis and poor response to treatment.

An advantage of our current study is that we have specifically measured the spatial distribution of antibody binding (which is directly related to the pattern of CEA expression), rather than less specific structural or metabolic image features, in two contrasting human colorectal metastatic tumour models in live mice; models for which we have prior knowledge of the likely microscopic distribution from previous studies that used more complex methodology directly on tumour tissue (El Emir *et al*, 2007). Our study shows the potential for texture analysis of medical images to non-invasively provide additional information related to

tumour phenotype and to provide novel quantitative imaging biomarkers that may predict or measure treatment response to radioimmunotherapy. Patients who are treated with radioimmunotherapeutics may have a SPECT scan prior to treatment with radiolabelled antibody with the possibility of a series of SPECT scans during therapy as the bound radiolabelled antibody persists in the tumour over time. The data from these reconstructed images can be used to estimate the dose distribution that the patient is receiving, but in addition, have the potential to provide information about how the cancer is responding and also how the distribution of the antigen target that is remaining in dead or dying tumour deposits is changing. Although ^{125}I -iodine is routinely used for pre-clinical SPECT imaging, and in our hands generated good quality SPECT images, the low energy gamma rays of ^{125}I -iodine render it unsuitable for quantitative SPECT imaging because of attenuation and scattering. We therefore envisage that further translation of these studies into the clinic will require the use of alternative isotopes such as ^{123}I -iodine for SPECT or ^{124}I -iodine for positron emission tomography. This study demonstrates the complexity involved in texture analysis, and supports the need for further correlative studies in order to determine the biological correlates of heterogeneity in other radiological imaging methods, and to further investigate the potential use of texture analysis methods in the development of novel imaging biomarkers.

In conclusion, texture analysis of ^{125}I -A5B7 SPECT is able to measure the greater spatial heterogeneity of CEA distribution in poorly differentiated liver metastases and a reduction in heterogeneity after anti-vascular treatment in these poorly differentiated tumours.

ACKNOWLEDGEMENTS

We acknowledge support from the NIHR Biomedical Research Centres of University College London Hospitals NHS Foundation Trust, and Guys & St Thomas' NHS Trust in partnership and Kings College London, and King's College London and UCL Comprehensive Cancer Imaging Centre funded by the CRUK and EPSRC in association with the MRC and DoH (England) and Cancer Research UK Research Centre (UCL Cancer Institute). We acknowledge OXiGENE for kindly supplying the drug CA1P (OXi4503).

CONFLICT OF INTEREST

The authors declare no conflict of interest.

REFERENCES

Al-Kadi OS, Watson D (2008) Texture analysis of aggressive and nonaggressive lung tumour CE CT images. *IEEE Trans Biomed Eng* **55**: 1822–1830.

Asselin MC, O'Connor JP, Boellaard R, Thacker NA, Jackson A (2012) Quantifying heterogeneity in human tumours using MRI and PET. *Eur J Cancer* **48**: 447–455.

Castellano G, Bonilha L, Li LM, Cendes F (2004) Texture analysis of medical images. *Clin Radiol* **59**: 1061–1069.

Chicklore S, Goh V, Siddique M, Roy A, Marsden PK, Cook GJ (2013) Quantifying tumour heterogeneity in 18F-FDG PET/CT imaging by texture analysis. *Eur J Nucl Med Mol Imaging* **40**: 133–140.

Cook GJ, Yip C, Siddique M, Goh V, Chicklore S, Roy A, Marsden PK, Ahmad S, Landau D (2013) Are pretreatment 18F-FDG PET tumour textural features in non-small cell lung cancer associated with response and survival after chemoradiotherapy? *J Nucl Med* **54**: 19–26.

Davnull F, Yip CS, Ljungqvist G, Selmi M, Ng F, Sanghera B, Ganeshan B, Miles KA, Cook GJ, Goh V (2012) Assessment of tumour heterogeneity: an emerging imaging tool for clinical practice? *Insights Imaging* **3**: 573–589.

Eary JF, O'Sullivan F, O'Sullivan J, Conrad EU (2008) Spatial heterogeneity in sarcoma 18F-FDG uptake as a predictor of patient outcome. *J Nucl Med* **49**: 1973–1979.

El Emir E, Qureshi U, Dearling JL, Boxer GM, Clatworthy I, Folarin AA, Robson MP, Nagl S, Konerding MA, Pedley RB (2007) Predicting response to radioimmunotherapy from the tumour microenvironment of colorectal carcinomas. *Cancer Res* **67**: 11896–11905.

El Naqa I, Grigsby P, Apte A, Kidd E, Donnelly E, Khullar D, Chaudhari S, Yang D, Schmitt M, Laforest R, Thorstad W, Deasy JO (2009) Exploring feature-based approaches in PET images for predicting cancer treatment outcomes. *Pattern Recognit* **42**: 1162–1171.

Folarin AA, Konerding MA, Timonen J, Nagl S, Pedley RB (2010) Three-dimensional analysis of tumour vascular corrosion casts using stereoisomeric and micro-computed tomography. *Microvasc Res* **80**: 89–98.

Ganeshan B, Goh V, Mandeville HC, Ng QS, Hoskin PJ, Miles KA (2013) Non-small cell lung cancer: histopathologic correlates for texture parameters at CT. *Radiology* **266**: 326–336.

Goh V, Sanghera B, Wellsted DM, Sundin J, Halligan S (2009) Assessment of the spatial pattern of colorectal tumour perfusion estimated at perfusion CT using two-dimensional fractal analysis. *Eur Radiol* **19**: 1358–1365.

Goh V, Ganeshan B, Nathan P, Juttla JK, Vinayan A, Miles KA (2011) Assessment of response to tyrosine kinase inhibitors in metastatic renal cell cancer: CT texture as a predictive biomarker. *Radiology* **261**: 165–171.

Haralick RM, Shanmuga K, Dinstein I (1973) Textural features for image classification. *IEEE Trans Syst Man Cybern* **3**: 610–621.

Henriksson E, Kjellen E, Wahlberg P, Ohlsson T, Wennerberg J, Brun E (2007) 2-Deoxy-2-(18F) fluoro-D-glucose uptake and correlation to intratumoural heterogeneity. *Anticancer Res* **27**: 2155–2159.

Howarth P, Ruger S (2004) Evaluation of texture features for content-based image retrieval. In *Image and Video Retrieval*, Enser P. (ed), pp 326–334. Springer-Verlag: Berlin.

Lankster KJ, Maxwell RJ, Pedley RB, Dearling JL, Qureshi UA, El-Emir E, Hill SA, Tozer GM (2007) Combretastatin A-4-phosphate effectively increases tumour retention of the therapeutic antibody, 131I-A5B7, even at doses that are sub-optimal for vascular shut-down. *Int J Oncol* **30**: 453–460.

Meyer T, Gaya AM, Dancey G, Stratford MR, Othman S, Sharma SK, Wellsted D, Taylor NJ, Stirling JJ, Poupard L, Folkes LK, Chan PS, Pedley RB, Chester KA, Owen K, Violet JA, Malaroda A, Green AJ, Buscombe J, Padhani AR, Rustin GJ, Begent RH (2009) A phase I trial of radioimmunotherapy with 131I-A5B7 anti-CEA antibody in combination with combretastatin-A4-phosphate in advanced gastrointestinal carcinomas. *Clin Cancer Res* **15**: 4484–4492.

Parikh J, Selmi M, Charles-Edwards G, Glendenning J, Ganeshan B, Verma H, Mansi J, Harries M, Tutt A, Goh V (2014) Changes in primary breast cancer heterogeneity may augment early MRI assessment of response to neoadjuvant chemotherapy. *Radiology* **272**: 100–112.

Rajkumar VS, Boxer G, Robson M, Muddle J, Papastavrou Y, Pedley RB (2014) A comparative study of PDGFR inhibition with imatinib on radiolabeled antibody targeting and clearance in two pathologically distinct models of colon adenocarcinoma. *Tumour Biol* **33**: 2019–2029.

Tixier F, Le Rest CC, Hatt M, Albarghach N, Pradier O, Metges JP, Corcos L, Visvikis D (2011) Intratumour heterogeneity characterized by textural features on baseline 18F-FDG PET images predicts response to concomitant radiochemotherapy in esophageal cancer. *J Nucl Med* **52**: 369–378.

Tixer F, Hatt M, Cheze Le Rest C, Le Pogam A, Corcos L, Visvikis D (2012) Reproducibility of tumor uptake heterogeneity characterisation through textural feature analysis in 18F-FDG PET. *J Nucl Med* **53**: 1–8.

Workman P, Balmain A, Hickman JA, McNally NJ, Rohas AM, Mitchison NA, Pierrepont CG, Raymond R, Rowlatt C, Stephens TC (1988) UKCCCR guidelines for the welfare of animals in experimental neoplasia. *Lab Anim* **22**: 195–201.

Yu H, Caldwell C, Mah K, Poon I, Balogh J, MacKenzie R, Khaouam N, Tirona R (2009) Automated radiation targeting in head-and-neck cancer using region-based texture analysis of PET and CT images. *Int J Radiat Oncol Biol Phys* **75**: 618–625.

This work is published under the standard license to publish agreement. After 12 months the work will become freely available and the license terms will switch to a Creative Commons Attribution-NonCommercial-Share Alike 4.0 Unported License.

APPENDIX 1

Appendix Table 1. Imaging heterogeneity parameters		
Uniformity	$\sum_i \sum_j \{p(i,j)\}^2$ <p>i, j is the voxel value in region of interest and $p(i,j)$ the probability of the occurrence of that voxel value.</p>	Measures the sum of squared elements in the matrix. Uniformity = 1 for a constant image.
Homogeneity	$\sum_i \sum_j \frac{p(i,j)}{1+(i-j)^2}$	Measures the closeness of the distribution of elements in the matrix to the diagonal.
Contrast	$\sum_{n=0}^{N_g-1} n^2 \left\{ \sum_{i=1}^{N_g} \sum_{j=1}^{N_g} p(i,j), \text{ where } i-j = n \right\}$ <p>N_g - number of distinct grey levels in the quantised image</p>	Measures contrast or local intensity variation and favours contributions from $p(i, j)$ away from the diagonal, that is, $i \neq j$.
Entropy	$-\sum_i \sum_j p(i,j) \log(p(i,j))$	A measure of randomness. Inhomogeneous textures have high entropy, whereas homogeneous textures will have low entropy.